



## Tuning Mechanical Properties of Nanocomposites with Bimodal Polymer Bound Layers

Journal:	<i>RSC Advances</i>
Manuscript ID:	RA-COM-07-2014-007157.R1
Article Type:	Communication
Date Submitted by the Author:	22-Sep-2014
Complete List of Authors:	Akcora, Pinar; Stevens Institute of Technology, Chemical Engineering & Materials Science Senses, Erkan; Stevens Institute of Technology, Chemical Engineering & Materials Science

## **Tuning Mechanical Properties of Nanocomposites with Bimodal Polymer Bound Layers**

**Erkan Senses and Pinar Akcora**

Department of Chemical Engineering and Materials Science

Stevens Institute of Technology, Hoboken, NJ 07030 USA

Mechanical properties of polymer nanocomposites can be enhanced by increasing nanoparticle loadings or by changing dispersion states. We present that a bound layer composed of short and long chains can be exploited to regulate the elastic modulus of bulk polymer nanocomposites within two orders of magnitude. The bound layer thickness on particles with high coverage of long chains is reduced with oscillatory deformation in a model attractive nanocomposite system. Reversibility of bound layer is, thus, possible for the short chains in the interphase. Compositional dynamic heterogeneity in the interphase has subsequent effects on the fragility of composites. With increasing amount of adsorbed long chains, fragility index systematically improves from moderate to high values. Our results suggest that the interphase layer between adsorbed chains and free matrix directly governs the reinforcement in poly(methyl methacrylate)-silica nanocomposites and can be dynamically altered under large shear.

## INTRODUCTION

Dynamic mechanical properties of polymer nanocomposites (PNCs) have been the focus of extensive research as the addition of small amount of fillers dramatically alters the viscoelastic behavior<sup>1,2,3,4</sup>. Performance of PNCs is primarily determined by interactions between particles and polymer, which controls the state of particle dispersion and the polymer dynamics around fillers. It is known that attractive interactions between particle and polymer slow down the mobility of chains, forming a ~1-4 nm thick bound layer<sup>5,6,7</sup>. Adsorption experiments have shown this bound layer is irreversible<sup>8</sup> and its dynamics can be measured in nuclear magnetic resonance (NMR)<sup>9,10</sup> and neutron spin-echo (NSE) spectroscopy<sup>11</sup>. Dynamics in the interphase region of polymer matrix and fillers has attracted much attention in recent years as entanglement density and glass-transition temperature change within confined media<sup>12,11,13,14,15,16</sup>. It has been shown in dynamic measurements that confinement of chains near particles can translate into the bulk phase through strong topological interactions<sup>11</sup>. This confined layer consists of a mobile layer on the surface, and an interphase which interacts with the adsorbed chains and melt matrix<sup>11</sup>. Inelastic neutron scattering experimental findings of Richter *et al.*<sup>17</sup> showed the end group effect on dynamics of bound PEG chains. They reported that while OH-ended chains were strongly adsorbed on particles and followed Rouse dynamics for grafted chains, CH<sub>3</sub>-terminated PEG chains were weakly adsorbed and led to a 1-nm thick bound layer which was found to be very mobile<sup>17</sup>.

In this work, we alter the effective interphase with the adsorption of bimodal chains on nanoparticle surfaces and examine the role of adsorbed layer on mechanical properties of poly(methyl methacrylate)-silica (PMMA-SiO<sub>2</sub>) nanocomposites. The interfacial layer effect has been studied recently on composites of polymer-grafted nanoparticles by Schadler *et al.*<sup>18</sup>. Well-dispersion was achieved in the

allophobic dewetting regime with bimodal brushes. This finding then led them to study the role of matrix-brush entanglement on thermomechanical properties<sup>18</sup>. At first sight, the problem of interfacial effect between grafted and free chains may look analogous to our work in which the interphases are between bare particles and adsorbed bimodal chains. In our system, however, bimodal chains are used to alter bound layer interactions between bare nanoparticles which can tune the physical properties of composites and also can be prepared easily as opposed to grafting methods applied to nanoparticles<sup>19</sup>. Adsorption of homopolymers<sup>5,20</sup> or diblock copolymers<sup>21</sup> on bare has been attracting more attention as a new strategy to disperse nanoparticles effectively in polymer matrices for their practical processibility.

Here, we demonstrate that by adsorbing bimodal blends of very short ( $\ll$  entanglement molecular weight,  $M_e$  of PMMA: 12.5 kg/mol<sup>22</sup>) and long polymer chains ( $> M_e$ ), the bound layer interactions can be physically modified from weak to strong within identical dispersion states. Additionally, we examine the mechanical consequences of bound layers at different compositions in attractive nanocomposites. Large amplitude oscillatory shear (LAOS) experiments on composites reveal that entanglements change within a bound layer<sup>20</sup>. In our past work, we have shown that loops and tails in the interfacial layer of PMMA-SiO<sub>2</sub> nanocomposite can be dynamically altered in LAOS runs<sup>20</sup>. An interesting finding was that as sample rests between two deformation cycles, matrix chains entangled more densely with the adsorbed chains, and led to large increases in elastic modulus compared to the deformed unfilled polymer. This work now aims to reveal the effect of entanglements within this interphase by changing its composition on the mechanical and glassy properties of nanocomposites.

## EXPERIMENTAL

### Materials

PMMA's of different molecular weights were synthesized by ATRP polymerization<sup>23</sup> using p-toluenesulfonyl chloride (TsCl) initiator, CuBr-CuBr<sub>2</sub> catalyst system with 2,2'-bipyridine in toluene at 70 °C. Colloidal SiO<sub>2</sub> nanoparticles (13 nm and 55 nm diameters) in methyl ethyl ketone were supplied by Nissan Chemicals America and used as received. The specifications of our samples are listed in Table 1.

**Table 1: Specifications of nanoparticles adsorbed with varying polymer blend compositions.**

molecular weight		volume fraction of long chains in blends $\Phi_L$	SiO <sub>2</sub>	
$\overline{M}_n$ [kg/mol] (Dispersity, $\Delta$ )			Size [nm]	wt %
96 (1.12)	4.3 (1.13)	1, 0.8, 0.5, 0.2, 0	13, 55	15
68 (1.05)	2.6 (1.13)	1, 0.95, 0.85, 0.7, 0.3, 0	55	30
12 (1.15)	2.6 (1.13)	1, 0.8, 0.5, 0.2, 0	55	30

**Adsorbed bimodal chains on nanoparticles:** Bimodal polymer blend solutions were prepared in acetonitrile (at 40 mg/mL) with varying long chain compositions. Blend solutions were mixed with nanoparticles at 30 wt% using a bath sonicator for 30 min. Solutions were stirred vigorously for 2 h and were immediately poured into Teflon dishes and evaporated overnight. Films were then annealed under vacuum at 150 °C for 3 days and at 180 °C for 2 h to ensure complete removal of solvent. Nanocomposites were then redissolved in acetonitrile and nanoparticles with bound polymer were recollected by centrifugation at 11,000 rpm for 5 min. Washing process was repeated 3 times to ensure all unbound chains were removed.

**Bound layer characterization:** DLS measurements were carried out with a Zetasizer NanoS (Malvern Instruments) at particle concentration of ~1 mg/mL in acetonitrile to measure the hydrodynamic

thickness of adsorbed layer. Measurement duration was 11 s, and data were averaged over 10 runs. TGA measurements were performed on a Q50 TGA (TA Instruments) to determine the mass amount of adsorbed polymer. Measurements were performed under a constant flow of nitrogen of 20 mL/min at a heating rate of 20 °C/min, starting from 40 °C up to 580 °C, while pausing isothermally at 150 °C for 20 min to ensure samples were free of solvent and then finally incubated at 580 °C for 20 min.

**Fourier Transform Infra-Red characterization:** Dry samples were mixed with KBr powder and compression molded to obtain transparent uniform films. Absorption spectra were obtained using a Tensor 27 FTIR spectrometer (Bruker Optics) in the range of 400–4000  $\text{cm}^{-1}$  with 64 scans of 4  $\text{cm}^{-1}$  resolution.

**Nanocomposite preparation:** Polymer bound particles were mixed with PMMA ( $\overline{M}_n$ : 28 kg/mol,  $D$ : 1.15) and solution cast to form bulk films. Films were then annealed for 3 days at 150 °C and 2 h at 180 °C under vacuum to remove any residual solvent.

**Nanoparticle structural characterization:** Films were microtomed into ~100 nm slices with a diamond knife at room temperature and examined by transmission electron microscopy (FEI CM20 FE S/TEM) at 200 keV. SAXS measurements were performed at Beamline X27C at the National Synchrotron Light Source (NSLS), Brookhaven National Laboratory. Air background subtracted data

were fit to the Beaucage unified equation;  $I(q) = \sum_i A_i \exp[-q^2 R_{gi}^2 / 3] + B_i [(\text{erf}(\frac{qR_{gi}}{\sqrt{6}}))^3 / (q)]^p$ , where

$R_g$  is the radius of gyration, and  $p$  is the fractal dimension of the scattering objects and  $A_i$  and  $B_i$  are constants for the  $i^{\text{th}}$  structural level. One level fit was sufficient to describe the patterns.

**Rheological characterization:** Linear and non-linear tests were performed on a strain-controlled ARES-G2 (TA Instruments) with 8-mm stainless-steel parallel plate fixtures. Composite samples were molded with a vacuum assisted compression molder at 180 °C for 10 min and then annealed at 130 °C for 12 h prior to the measurements. Experiments were performed at 210 °C after 10 min equilibration

time. LAOS tests were performed at a fixed frequency of 1 rad/s and at strain amplitude 300%. Measurement time was 300 s and data was collected at 300 Hz sampling frequency. Sheared samples were quenched below  $T_g$  of PMMA in  $\sim 1$  min while the axial force is controlled within  $\pm 1$  N to prevent thermal strain. Data was analyzed by using MITLaos software as previously reported<sup>24</sup>.

**Glass transition and dynamic fragility:** Fragility and glass transition temperatures on composite films were determined by using Q100 DSC (TA Instruments). The samples were first heated to 175 °C for 5 min and then cooled down to 30 °C at different cooling rates ( $Q$ ) ranging from 0.2 to 30 °C/min followed by heating to 175 °C by standard heating rate of 10 °C /min. The glass transition temperatures ( $T_g$ ) were determined from the inflection point on the heating curves following the standard cooling rate  $Q_{std} = 20$  °C/min. The limiting fictive temperatures,  $T_f$ , were obtained from each heating scan by using the instrument software (Q-Advantage). The dynamic fragility index,  $m$ , was determined from the relationship,  $\ln(Q/Q_{std}) = m - mT_{f, std} / T_f$ , where  $T_{f, std}$  is the standard fictive temperature for  $Q_{std}$ <sup>25</sup>.

## RESULTS and DISCUSSION

### Bimodal chain adsorption on nanoparticles

We first studied the dispersion of bare nanoparticles in homopolymer blend matrices. Hydrogen bonding between oxygen atoms on PMMA and hydroxyl groups on SiO<sub>2</sub> favors the physical adsorption of polymer to nanoparticle surfaces. Polymer-solvent interactions govern the adsorption process. For example, samples prepared in MEK or THF, which are good solvents for PMMA, exhibited poor dispersion since solvent can displace chains on nanoparticles and impede the adsorption of chains (see Figure S1 and discussion in Supporting Information). We used acetonitrile, a  $\Theta$ -solvent for PMMA, in preparation of our composites as chains can adopt their ideal chain conformations in both solution and melt states<sup>26</sup>. We mixed SiO<sub>2</sub> nanoparticles in solutions of blend homopolymers (96 and 4.3 kg/mol

PMMA). TEMs in Figures 1a-b show individual dispersion of nanoparticles (13 nm and 55 nm in diameter, at 15 wt% loading) in 96-4.3 kg/mol blend matrix (50/50 vol/vol %). Figure 1c displays SAXS patterns for 13 nm nanoparticles in matrices with different blend compositions. Individually dispersed nanoparticles of  $\sim 7$  nm radius were obtained from low  $q$ -fitting, governed by the Guinier equation<sup>27</sup>:  $I(q) = I_0 \exp[-(qR_g)^2 / 3]$ . The scaling in the Porod regime,  $I(q) \propto q^{-4}$ , suggests particles are dispersed with sharp surfaces in all samples.

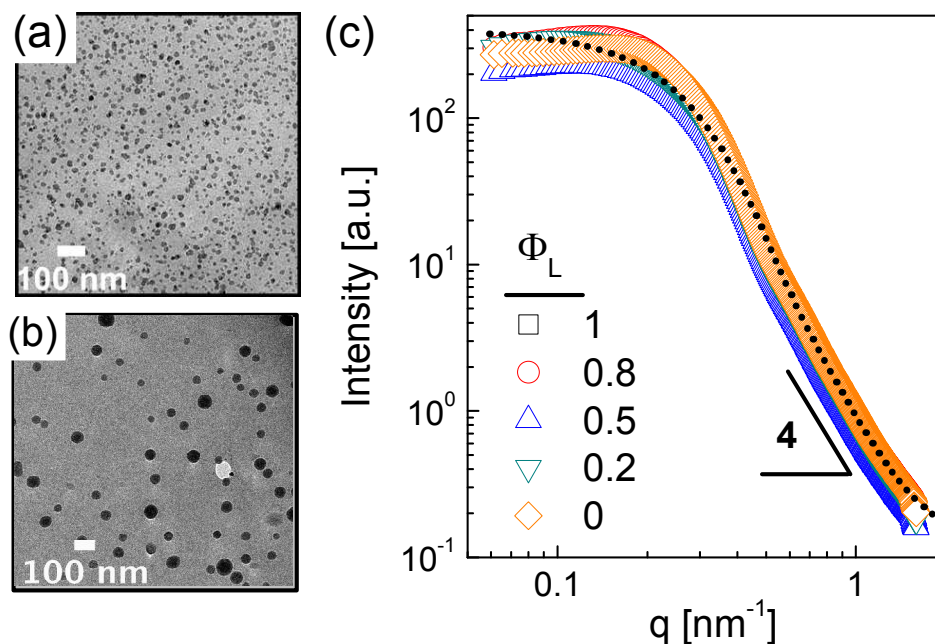


**Figure 1.** TEM images for (a) 13 nm and (b) 55 nm SiO<sub>2</sub> nanoparticles in matrix composed of 96 and 4.3 kg/mol PMMA homopolymers at 50/50 vol%. Images at low magnifications are presented in Figure S2. (c) SAXS patterns for nanocomposites with varying matrix compositions.  $\phi_L$  is the volume fraction of long chains in blend matrix. Dashed line is a Unified fit for a single level structure. Particle loading is 15 wt% in all composites.

Next, we dispersed bare particles in 68 and 2.6 kg/mol PMMA homopolymer mixtures for bimodal chain adsorption (see experimental for procedure). We used 55 nm nanoparticles in our composites

because the amount of adsorbed polymer on 55 nm particles is higher due to less curvature effect. Nanoparticles extracted from composites were analyzed in DLS and TGA (data shown in Figure S3) following the reported protocol<sup>5</sup>. It is evident that hydrodynamic sizes of polymer bound nanoparticles ( $h$ ) are larger than bound polymer thicknesses ( $t$ ), and both parameters systematically increase with the fraction of long chains (Figure 2). These results indicate that the composition of the bound layer changes by varying the fractions of long and short chains in the blend matrix.

Differences in desorption probabilities drives the well-known competitive adsorption of chains with different lengths on flat surfaces. It was shown by Dijt *et al.*<sup>28</sup> that kinetics of adsorption is primarily determined by transport of chains from dilute solution to the surface. Short chains that are adsorbed first are replaced by long chains eventually<sup>29,30</sup>. These studies on the preferential adsorption or exchange of long and short chains are in dilute solution limit. This mechanism does not apply in our system because particles are adsorbed in concentrated polymer solution. Granick *et al.*<sup>31</sup> showed that strongly adsorbing chains on surface can sterically pin weakly adsorbed ones, resulting in their extended life-time on surface. In the case of bimodal chain adsorption, the weakly adsorbed short chains can be pinned by the strongly adsorbed long polymers. This may create an additional entropic barrier to prevent desorption of the short chains.

It is also known that conformation of adsorbed chains from semi-dilute concentration or melt is the same as in solution<sup>32</sup>. Thus, the scaling for bound layers with the chain length,  $N^{1/2}C^{7/8}$ , at semi-dilute concentration is a reasonable argument and can be applied for the adsorbed amount of bimodal chains from their close-to semi-dilute concentration solutions. Virgiliis *et al.*<sup>33</sup> predicted that the amount of polymer adsorbed from melt scales with  $N^{1/2}$ , which agrees with the theoretical predictions by Fleer<sup>34</sup>. In our system with bimodal bound layer, thickness of bound layer also varies linearly with  $N_{ave}^{1/2}$  as shown in Figure 2.  $N_{ave}$  is defined as  $N_{ave} = \phi_L N_L + (1-\phi_L) N_S$ , where  $\phi_L$  is the volume fraction of long chains (68

kg/mol),  $N_L$  and  $N_S$  is the degree of polymerization for long chains and short chains (2.6 kg/mol), respectively.

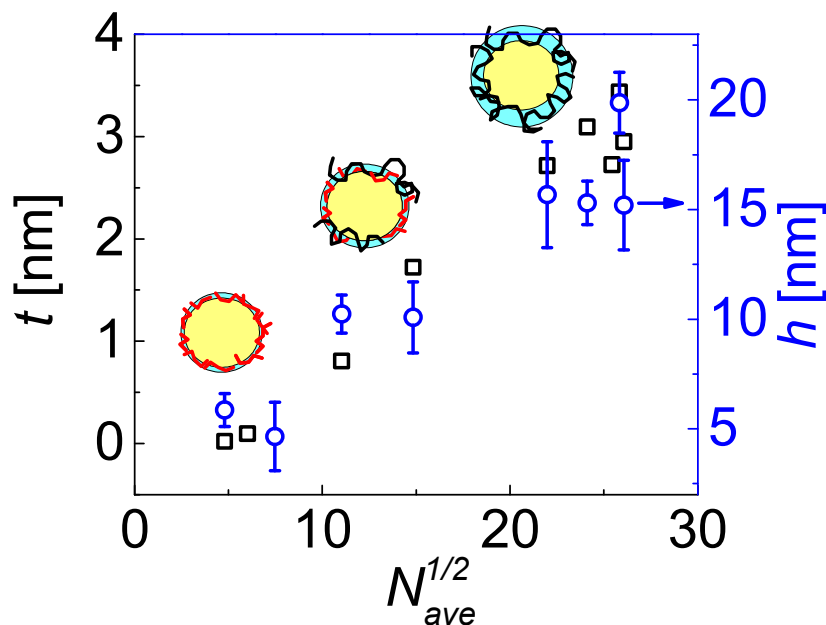


**Figure 2.** Bound layer thicknesses determined from TGA ( $t$ ) (black squares) and DLS ( $h$ ) (blue circles) as a function of  $N_{ave}^{1/2}$ . Cartoons represent the bound layer thickness variation with increasing coverage of long chains on particles.

Previous works have shown that boundary layer thicknesses obtained in DLS and TGA measurements are in agreement<sup>5</sup> with the theoretical predictions and scales as  $N^{1/2}$ . In our system, since polymer solution contains bimodal chains, it is essential to confirm the existence of short chains on extracted particles after series of washing and annealing steps. It is apparent that C=C resonance of end-group becomes apparent with the presence of short chains. Spectra of pure homopolymers are compared in the Supporting Information (Figure S4). By taking the area ratio of end-group in the short-chain signals (C=C in the aromatic ring) and C=O group of PMMA (Figure 3c), we show that the short chain amount decreases when the long chains in the blend decreases. Figure 3b shows the spectra of bare particles and bimodal PMMA adsorbed nanoparticles for C=O signal at  $1740\text{ cm}^{-1}$  of PMMA and C=C

signal at  $1652\text{ cm}^{-1}$  of TsCl. It is clear from the FTIR spectra and the DLS/TGA analysis that compositions of the bound layers on nanoparticles are determined by the composition of the bimodal matrix from which the chains are adsorbed.

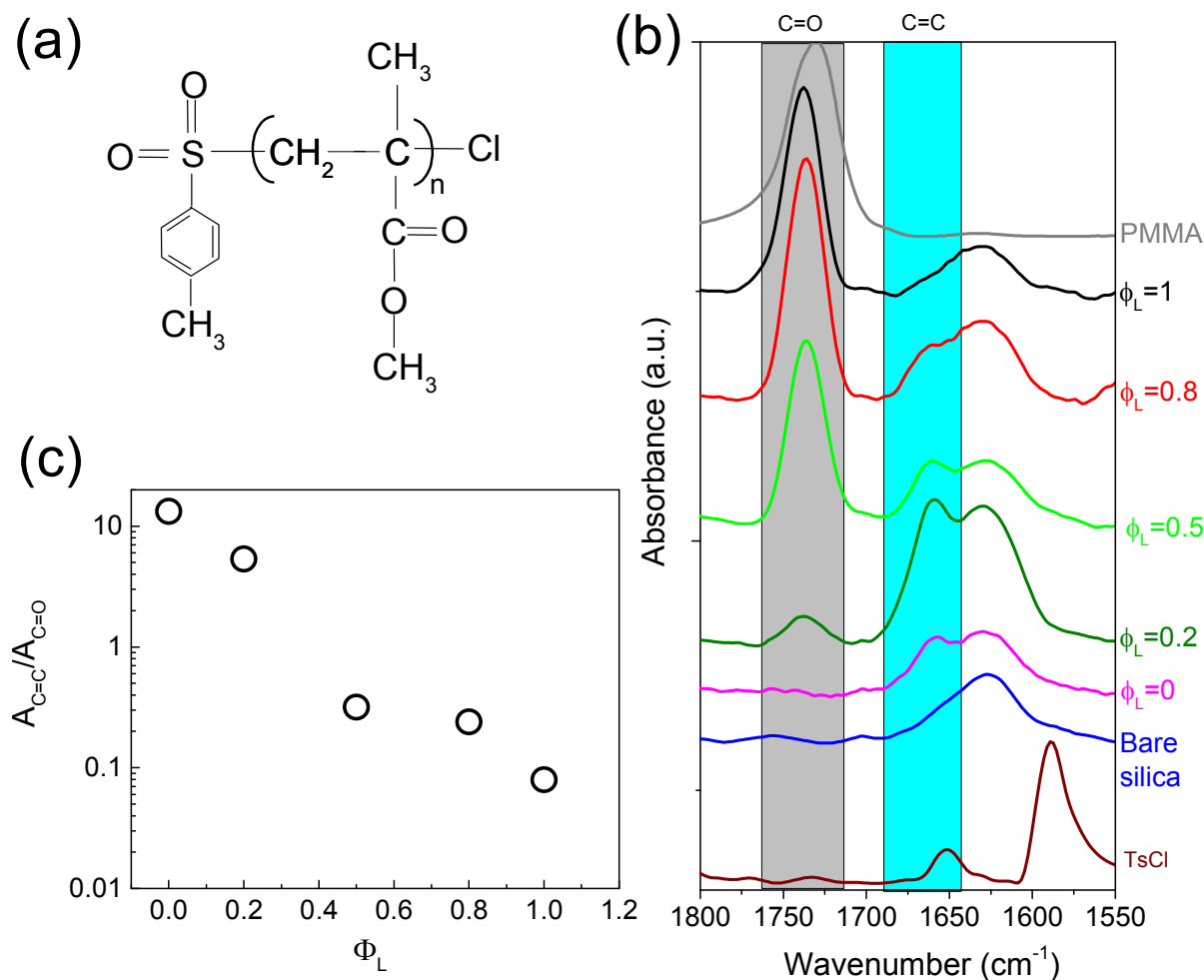


**Figure 3.** (a) Chemical structure of PMMA with its end groups. (b) FTIR spectra for bare 55-nm SiO<sub>2</sub> nanoparticles and bimodal PMMA chains (2.6 kg/mol and 150 kg/mol) adsorbed on nanoparticles with varying long chain fractions ( $\phi_L$ ). PMMA labeled spectrum in (b) is for 150 kg/mol. (c) Ratio of peak areas of C=C and C=O bands.

## Effects of bimodal adsorbed chains on mechanical properties of nanocomposites

The main focus of our work is to examine mechanical consequences of bimodal bound layers on nanoparticles in melts. Nanoparticles adsorbed with bimodal chains of 68 and 2.6 kg/mol PMMA homopolymers (samples in Figure 2) are redispersed in 28 kg/mol PMMA matrix. Matrix molecular weight is chosen carefully to be 28 kg/mol above entanglement molecular weight in order to observe the changes of relaxation times during deformation<sup>20</sup>. Dispersion state of nanoparticles adsorbed with bimodal chains in 28 kg/mol PMMA matrix is shown in Figure 4. It is expected that PMMA of 2.6 kg/mol is unable to form loops or entangle with matrix chains near the surface. Thus, changing the fraction of long adsorbed chains can control interfacial entanglement density, and hence rheological properties in attractive nanocomposites. Figure 4 shows the elastic modulus ( $G'$ ), loss modulus ( $G''$ ) and  $\tan\delta$  over four decades of angular frequencies for various bound layer compositions. The low frequency regime of  $G'$  clearly shows changes in equilibrium relaxation behavior upon increasing the loop concentration on filler surfaces. Elastic modulus is modified by two orders of magnitude with the increased amount of long chains in bound layers within the same dispersion state of fillers. Our study further reveals the effect of interfacial entanglements on tuning the rheological properties within the same particle dispersion and loading. We further analyzed the viscosity data of our well-dispersed particles. We obtained the zero shear viscosities ( $\eta_0$ ) by fitting a three-parameter Cross model (see SI and Figures S6-7 for fitting details). The reinforcement factors obtained at different  $\phi_L$  (i.e.  $\log(\eta_0(\phi_L) / \eta_{0,Matrix})$ ) are plotted against the hydrodynamic size of the particles ( $h$ ) (Figure S8). The linear dependence was extrapolated to  $h=0$  to obtain reinforcement of well-dispersed particles in the absence of adsorbed layer (forming a non-sticky particle case). The extrapolated value, 1.6, agrees reasonably well with the Guth prediction<sup>35</sup> ( $\eta/\eta_{Matrix}=1+2.5\phi+14.1\phi^2=1.84$  with  $\phi=0.17$  in our case) where the reinforcement is due to hydrodynamic contribution at high loadings. This result suggests that the

viscosity increase in attractive nanocomposites can be effectively altered with interfacial entanglements. To verify that reinforcement is a result of entanglements within the bound layer, we prepared a composite bound with 12 and 2.6 kg/mol chains at the same particle loading. Reinforcement is not observed in this system (Figure S9) because 12 kg/mol chains, which are smaller than entanglement molecular weight of PMMA, do not entangle.

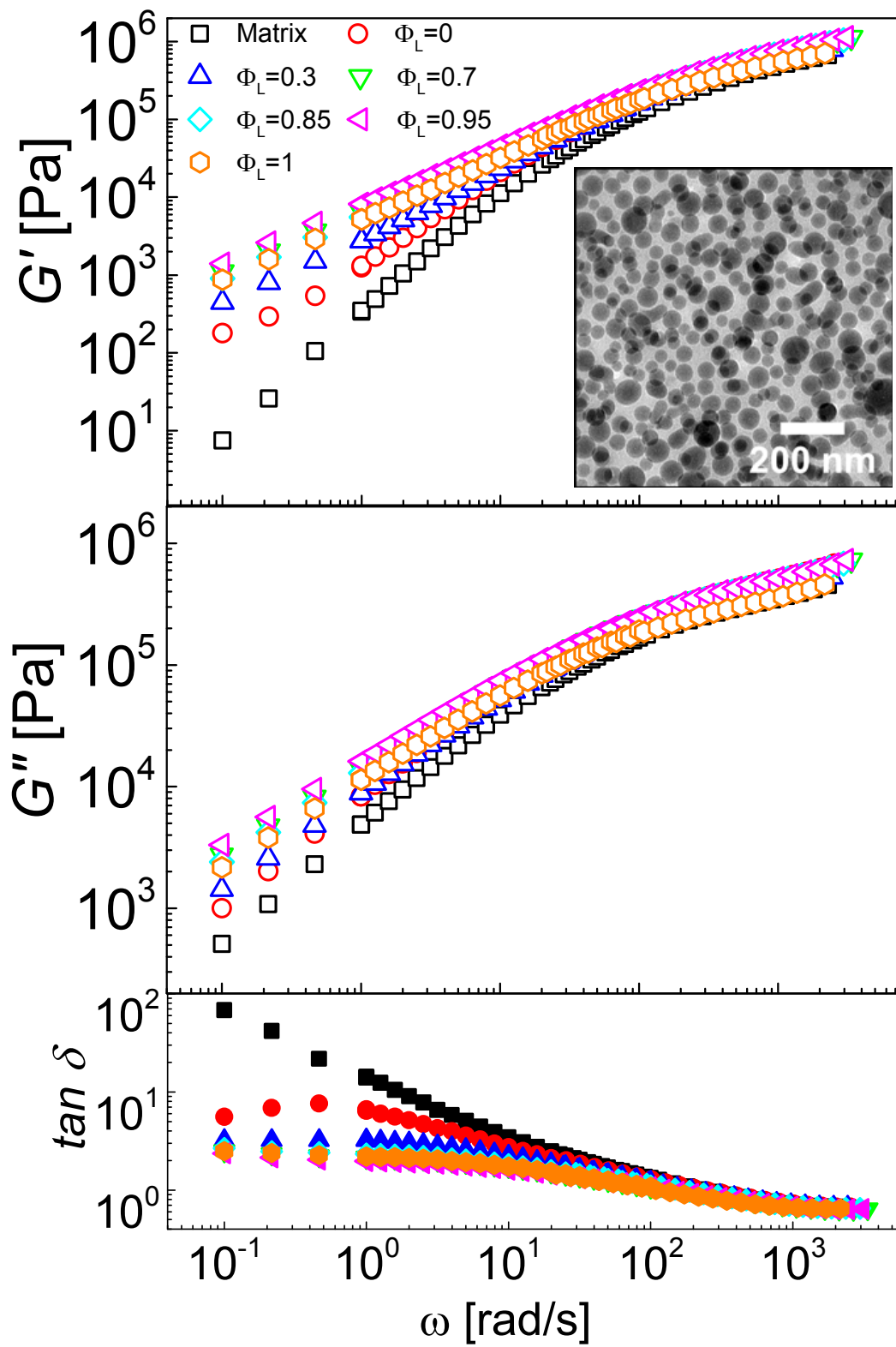


**Figure 4.** Linear elastic, loss moduli, and loss tangent of nanocomposites with particles adsorbed with a mixture of 68 and 2.6 kg/mol PMMA dispersed in 28 kg/mol PMMA matrix. Particle volume fraction,  $\phi_{\text{part}} = 0.17$  and  $T_{\text{ref}} = 210$  °C. The inset shows nanoparticle dispersion at 30 wt% (with  $\phi_{\text{L}} = 0.5$ ). TEM at lower magnification is displayed in Figure S5.

Next, we investigated the large shear response of bimodal chains adsorbed nanoparticles. In our previous work, we showed in PMMA-SiO<sub>2</sub> nanocomposite system that entanglement density around fillers can be altered with application of large amplitude oscillatory shear<sup>20</sup>. When the recovery of polymer modulus was monitored at rest, it was seen that composite stiffened after applying large strains, while the homopolymer recovered its initial modulus. During large-amplitude oscillatory deformations, chains can be desorbed and reabsorbed, and the loop concentration may increase, which can lead to a self-stiffening behavior after shear due to increased entanglement density at the interphase. Correspondingly, such attractive systems can display unusual mechanical responses if the entanglement density of the interfacial layer is altered in a controlled fashion. Here, we further substantiate the origin of the self-stiffening of attractive composites by only changing the concentration of the loops using bimodal adsorbed chains. We apply similar deformation protocol<sup>20</sup> (see experimental) to our composites and expect to see stiffening due to interphase effect formed by adsorbed bimodal chains. Samples were deformed for 300 s and then immediately quenched below  $T_g$ . Stress-response averaged from the last 5 cycles were analyzed. Stress-strain curves (Lissajous plots) for the matrix and composites (Figure 5a) present strengthening in non-linear regime. Total response is decomposed into its elastic and viscous components. Figure 5b shows the intra-cycle elastic stress-strain behavior of composites. It is evident that the average stress increases with the amount of long chains in the bound layer. Non-linear strain-stiffening<sup>24</sup>,  $G_L' / G_S'$ , determined from the ratio of the modulus in the limit of zero strain,  $G_S' =$

$\lim_{\gamma \rightarrow 0} (d\sigma/d\gamma)$ , and large-strain  $\gamma_0$ ,  $G_L' = \sigma(\gamma_0)/\gamma_0$ , shows a strong dependence on the composition of the bound layer (Figure 5d). Strain stiffening at large strain is due to stretching of the chains<sup>36</sup>, which is governed by the entanglements at the interphase as schematically represented in Figure 5c.

The entropic barrier for desorption of short chains can be overcome by large shear. By distorting the conformation of the long chains on surface, this barrier is reduced and desorption/readsorption can be facilitated by large shear. To examine the deformation effect on bound layer thickness, samples deformed at large strains were quenched below  $T_g$ , and particles were recollected. Figure 6 compares the bound layer thicknesses before and after deformation. TGA results indicate that the bound layer thickness is reduced at high coverage of long chains after deformation which suggests that number of loops increases with shear and enables the denser entanglements at interphases, resulting in the stiffening observed under shear. The bound layer thickness remains nearly the same with small fractions of short chains which may be readsorbed on surfaces easily during and after deformation. This result reveals that bound layer of short chains is more likely to be reversible compared to the readsorption of long chains.

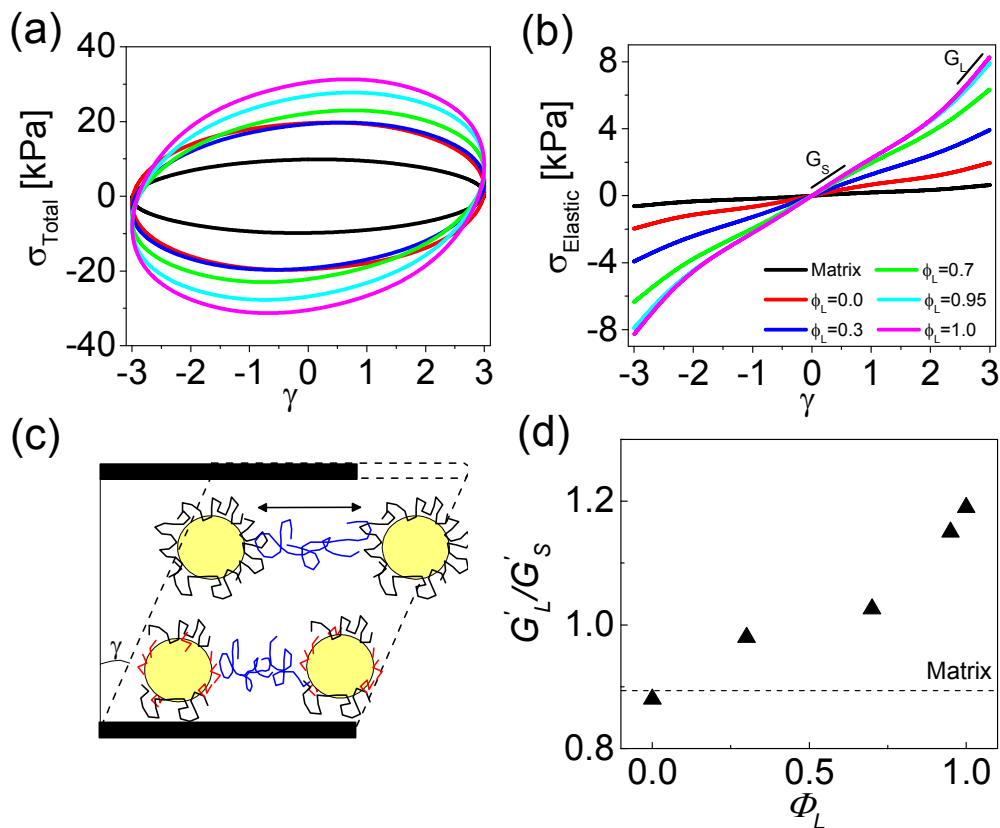


**Figure 5.** (a) Total stress-strain curves (Lissajous plots) for 28 kg/mol PMMA homopolymer and its composites containing SiO<sub>2</sub> nanoparticles (at 30 wt%) adsorbed with a mixture of 68 and 2.6 kg/mol PMMA at varying compositions. LAOS tests were performed at  $T = 210$  °C, with  $\gamma_0 = 3$  and  $\omega = 1$  rad/s. (b) Corresponding decomposed elastic stress-strain behavior of nanocomposites. Slopes presented are the moduli at the limit of zero-strain ( $G_S'$ ) and maximum-strain ( $G_L'$ ). (c) Schematic representation of chains stretching under large shear at different entanglement levels. (d) Strain-stiffening ( $G_L'/G_S'$ ) as a function of  $\phi_L$ .

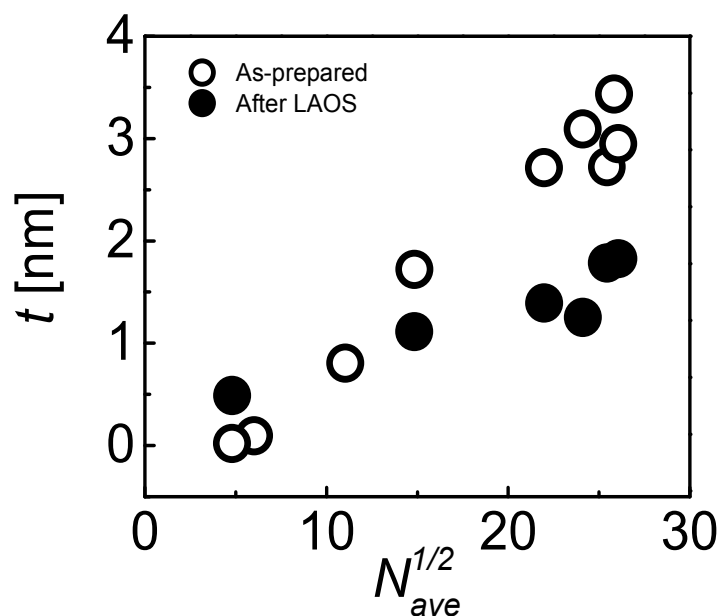


**Figure 6.** Bound layer thicknesses ( $t$ ) determined from TGA as a function of  $N_{ave}^{1/2}$  before (unfilled symbols) and after deformation (filled symbols).

### Effect of bound layer composition on glass transition and fragility

As the interphases become more heterogeneous by adsorption of bimodal polymer chains with different mobilities, the glassy behavior may also be altered. To understand the consequences of the enhanced dynamic properties and the interphase effect on thermal properties, we performed glass transition ( $T_g$ ) and fictive temperature ( $T_f$ ) measurements on composites. Figure S10 shows that  $T_g$  and  $T_f$  are not dependent on the bound layer thickness, which is consistent with small  $T_g$  changes reported for nanocomposites with attractive polymer-filler interactions<sup>37</sup>.  $T_g$  increase in attractive nanocomposites has been commonly observed in confined environments induced by nanoparticles<sup>38</sup>, however in our system particles do not form any confined regions since interparticle distance (ID)/ $2R_g$  ratio falls in the unconfined regime. Fragility index is a measure of deviations from Arrhenius type behavior in the

vicinity of glass transition and was shown to increase with monomer-surface interaction and particle loading<sup>39</sup>. We measured that with the adsorption of bimodal chains on particles, interphases become compositionally heterogeneous and dynamic fragility index increases from 115 to 168 (Figure 7). This behavior is attributed to the increased interfacial entanglements of long chains. According to Adam-Gibbs theory<sup>40</sup>, relaxations become increasingly cooperative and size of the cooperative rearranging regions (CRR) governs the behavior of liquid upon cooling. With the loop forming long chains on a surface, size of the CRR can be increased through entanglements in the interphase, thus composites become more fragile with  $\phi_L$ . We note the maximum in fragility is seen at  $\phi_L \sim 0.90$ , which may be explained with the additional dynamic heterogeneities created by the swelling of bound layer with short chains. Dilation of long chains with the short ones results in swelling of the entanglement tube which may result in longer loops on surface. This effect is more apparent in dilute regime of short chains since long chains will start disentangling if large amounts of short chains exist. Dynamic results suggest that using bimodal chains with small fraction of short chains on nanoparticle surfaces can improve the interfacial strength between matrix and fillers. Furthermore, the maximum observed at similar composition implies that elastic reinforcement in nanocomposite melts can be related to dynamic fragility, which are often thought to be unrelated. Further theoretical and experimental studies are needed to elucidate the effect of bimodal adsorbing chains on the glass-transition and fragility index.

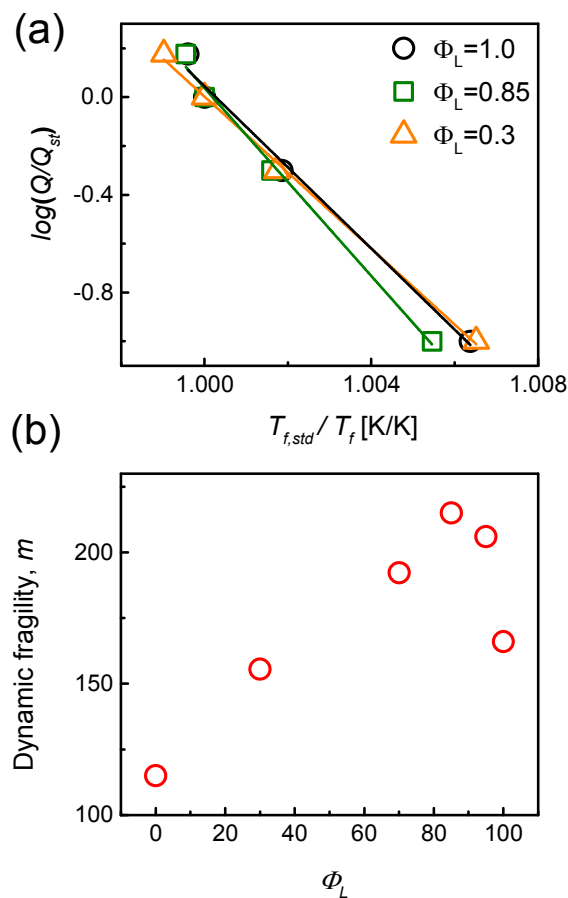


**Figure 7.** (a) Representative normalized cooling rate versus normalized fictive temperature plots are used to determine fragility index. (b) Change in dynamic fragility index with long chain concentration on nanoparticles.

## CONCLUSIONS

We showed on an attractive polymer nanocomposite system that the bound layer interactions are tuned upon adsorbing homopolymers of bimodal chain lengths on nanoparticles. Subsequent changes in interfacial entanglement density enhance the elastic properties of nanocomposites. While glass transition is not affected by dynamic heterogeneities created with bimodal chains on surfaces, the fragility index is varied systematically from moderate to high values. These results corroborate the consequences of

bound layer on mechanical and glassy properties of nanocomposites. Bimodal bound layers reveal the role of interphase layer on reinforcement mechanism and can further be used to modulate stiffness of polymer nanocomposites through shear-induced desorption/readsorption of chains.

## ACKNOWLEDGEMENTS

We acknowledge Stevens start-up funds. We also thank Yang Jiao for her help on SAXS experiments. Portions of this work were performed at Beamline X27C at the National Synchrotron Light Source (NSLS), Brookhaven National Laboratory. NSLS is supported by the U.S. Department of Energy, Office of Science, Office of Basic Energy Sciences, under Contract No. DE-AC02-98CH10886.

## REFERENCES

- (1) Sternstein, S.; Zhu, A.-J. *Macromolecules* **2002**, *35*, 7262.
- (2) Zhang, Z. P.; Liu, J. H.; Liao, L. B.; Xiao, C. B.; Li, R.; Zhang, Z. P. *Key Engineering Materials* **2007**, *334*, 833.
- (3) Xiao, C. B.; Zhang, Z. P.; Liu, J. H.; Li, R.; Zhang, Z. P. *Key Engineering Materials* **2007**, *334*, 865.
- (4) Zhang, Q.; Archer, L. A. *Langmuir* **2002**, *18*, 10435.
- (5) Jouault, N.; Moll, J. F.; Meng, D.; Windsor, K.; Ramcharan, S.; Kearney, C.; Kumar, S. K. *ACS Macro Letters* **2013**, *2*, 371.
- (6) Harton, S. E.; Kumar, S. K.; Yang, H.; Koga, T.; Hicks, K.; Lee, H.; Mijovic, J.; Liu, M.; Vallery, R. S.; Gidley, D. W. *Macromolecules* **2010**, *43*, 3415.
- (7) Sargsyan, A.; Tonoyan, A.; Davtyan, S.; Schick, C. *European Polymer Journal* **2007**, *43*, 3113.
- (8) O'Shaughnessy, B.; Vavylonis, D. *Physical Review Letters* **2003**, *90*, 056103/1.
- (9) Kim, S. Y.; Meyer, H. W.; Saalwächter, K.; Zukoski, C. F. *Macromolecules* **2012**, *45*, 4225.
- (10) Papon, A.; Saalwächter, K.; Schäler, K.; Guy, L.; Lequeux, F.; Montes, H. *Macromolecules* **2011**, *44*, 913.
- (11) Krutyeva, M.; Wischniewski, A.; Monkenbusch, M.; Willner, L.; Maiz, J.; Mijangos, C.; Arbe, A.; Colmenero, J.; Radulescu, A.; Holderer, O.; Ohl, M.; Richter, D. *Physical Review Letters* **2013**, *110*.
- (12) Ciprai, D.; Jacob, K.; Tannenbaum, R. *Macromolecules* **2006**, *39*, 6565.
- (13) Rittigstein, P.; Priestley, R. D.; Broadbelt, L. J.; Torkelson, J. M. *Nature Materials* **2007**, *6*, 278.
- (14) Papon, A.; Montes, H.; Hanafi, M.; Lequeux, F.; Guy, L.; Saalwächter, K. *Physical Review Letters* **2012**, *108*.
- (15) Kim, S. Y.; Zukoski, C. F. *Macromolecules* **2013**, *46*, 6634.
- (16) Li, Y.; Kröger, M.; Liu, W. K. *Soft Matter* **2014**, *10*, 1723.

- (17) Glomann, T.; Schneider, G.; Allgaier, J.; Radulescu, A.; Lohstroh, W.; Farago, B.; Richter, D. *Physical review letters* **2013**, *110*, 178001.
- (18) Natarajan, B.; Neely, T.; Rungta, A.; Benicewicz, B. C.; Schadler, L. S. *Macromolecules* **2013**, *46*, 4909.
- (19) Guan, L.-Z.; Wan, Y.-J.; Gong, L.-X.; Yan, D.; Tang, L.-C.; Wu, L.-B.; Jiang, J.-X.; Lai, G.-Q. *Journal of Materials Chemistry A* **2014**, *2*, 15058.
- (20) Senses, E.; Akcora, P. *Macromolecules* **2013**, *46*, 1868.
- (21) Jouault, N.; Lee, D.; Zhao, D.; Kumar, S. K. *Advanced Materials* **2014**, *26*, 4031.
- (22) Fetters, L.; Lohse, D.; Colby, R. In *Physical properties of polymers handbook*; Springer, 2007.
- (23) Matyjaszewski, K.; Xia, J. *Chemical Reviews* **2001**, *101*, 2921.
- (24) Ewoldt, R. H.; Hosoi, A.; McKinley, G. H. *Journal of Rheology (1978-present)* **2008**, *52*, 1427.
- (25) Wang, L.-M.; Velikov, V.; Angell, C. *The Journal of chemical physics* **2002**, *117*, 10184.
- (26) Rubinstein, M.; Colby, R. H. *Polymer physics*; OUP Oxford, 2003.
- (27) Guinier, A. *X-ray diffraction: in crystals, imperfect crystals, and amorphous bodies*; Courier Dover Publications, 2013.
- (28) Dijt, J. C.; Stuart, M. A. C.; Fleer, G. J. *Macromolecules* **1994**, *27*, 3219.
- (29) Fu, Z.; Santore, M. M. *Macromolecules* **1998**, *31*, 7014.
- (30) Santore, M. M. *Current opinion in colloid & interface science* **2005**, *10*, 176.
- (31) Johnson, H. E.; Granick, S. *SCIENCE*. **1992**, *255*, 966.
- (32) Guiselin, O. *EPL (Europhysics Letters)* **1992**, *17*, 225.
- (33) De Virgiliis, A.; Milchev, A.; Rostiashvili, V.; Vilgis, T. *The European Physical Journal E: Soft Matter and Biological Physics* **2012**, *35*, 1.
- (34) Scheutjens, J.; Fleer, G. *Journal of Physical Chemistry* **1979**, *83*, 1619.
- (35) Mooney, M. *Journal of colloid science* **1951**, *6*, 162.
- (36) Senses, E.; Akcora, P. *Journal of Polymer Science Part B: Polymer Physics* **2013**, *51*, 764.
- (37) Moll, J.; Kumar, S. K. *Macromolecules* **2012**, *45*, 1131.
- (38) Srivastava, S.; Basu, J. K. *Physical Review Letters* **2007**, *98*.
- (39) Starr, F. W.; Douglas, J. F. *Physical review letters* **2011**, *106*, 115702.
- (40) Adam, G.; Gibbs, J. H. *The journal of chemical physics* **1965**, *43*, 139.